ELSEVIER

Polymer 42 (2001) 8179–8195

polymer

www.elsevier.nl/locate/polymer

Processing–structure–properties relationship of multilayer films. 1. Structure characterization

Xiaomin Zhang[a,*], Abdellah Ajji[a], Verilhac Jean-Marie[b]

[a]*Industrial Materials Institute, National Research Council Canada, 75, Boulevard De Mortagne, Boucherville, Quebec, Canada J4B 6Y4*
[b]*ITECH, 7 Pagece Street, 69 Soo Bron, France*

Received 28 December 2000; received in revised form 15 April 2001; accepted 18 April 2001

Abstract

Low density polyethylene (LDPE)/poly(ethylene terephthalate) (PET) multilayer films with and without a reactive tie layer were prepared by blowing process. The layers contents were fixed and the parameters evaluated were blow-up ratio (BUR), draw-down ratio (DDR) and frost-line height (FL). Their effect on the structure was studied. No crystallinity for the PET layer was induced by the blowing process. The orientation of the multilayer films was characterized by birefringence and infrared spectroscopy (FTIR). The measured birefringence showed a negligible orientation for PET layer, and the LDPE layer oriented mainly along the machine direction. FTIR characterization also showed a negligible orientation for PET layer, and for LDPE layer, the crystalline *a*-axis tended toward machine direction, crystalline *b*-axis located in transverse–normal plane with no orientation for the amorphous phase. The lamellar arrangement of LDPE layer with respect to machine direction was obtained by dissolving the amorphous phase in solution of potassium permanganate in a mixture of equal volumes of orthophosphoric and sulfuric acid. The crystallization of oriented LDPE melts produced a morphology consisting of rows of lamellar crystals aligned parallel to the machine direction at higher draw-down ratio. It was not always of the row-nucleated type, the exact morphology patterns greatly depended on the distribution of the crystalline *a*-axis and *b*-axis orientation, which in turn was dependent on DDR, BUR and frost-line height.

Keywords: Multilayer films; Blowing process; Orientation

1. Introduction

In the film blowing process, the molten polymer is extruded through an annular die and the air is forwarded from the center of die to form a bubble. The molten tube leaving the die is stretched upwards by the nip rolls, at the same time cooling is performed through an air ring which directs air to the outside surface of the bubble and thus will affect closely molecular relaxation and crystallinity. The properties of blown films are determined by a complex relationship involving materials properties, the structure developed after the polymer exits the die where the bubble undergoes orientation, and crystallization and morphology development. The blow-up ratio (ratio of final diameter of bubble to the die diameter), draw-down ratio (DDR) (ratio of take-up speed to the velocity of the polymer as it exits the die) and the so called process time (the time between the die exit and the frost line) which characterizes how fast the stretching is performed, are the important parameters that control the amount of orientation with respect to the transverse and machine directions, and that determine the development of the crystal lamellar morphology and degree of crystallinity.

Some investigations [1–13] studied the kinematics, such as bubble shape, bubble temperature profile, strain history, cooling process and numerical calculations of air flow and heat transport of the blown films, and their relationship to film properties. Most studies [14–25] focused on the effect of processing parameters (BUR and DDR) on the structure and physical properties of polyethylene monolayer films.

The multilayer films have been paid more attention and showed high growth rate because of their cost/performance ratio. Compared with monolayer blown films, relatively few studies concerned blown multilayer films [26–29]. The situation of the multilayer films is complicated by the interfacial instabilities [26] and interlayer adhesion [28,29], for example, the simple addition of an individual layer to the ethylene- vinyl alcohol (EVOH)/HDPE multilayer films was shown to be not sufficient to design new multilayer film structure [28,29]. The application of a reactive compatibilizer (tie layer) on multilayer films has been reported

* Corresponding author.
E-mail address: zhang.xiaomin@nrc.ca (X. Zhang).

0032-3861/01/$ - see front matter
PII: S0032-3861(01)00301-9

recently [30,31]. Multilayer films with alternating layers were prepared with a system consisting of two or more than two extruders, a coextrusion block and a die assembly. The reactive tie layer has been shown to be effective to increase adhesion [30] and to prevent delamination of the multilayer film [31]. However, structure development, application of the reactive tie layer and possible interfacial effect for the blown multilayer films remain under studied.

The orientation of the crystalline and amorphous phases control the structure and performance of blown films. It is thus very important to be able to determine orientation characteristics of the blown films. The uniaxial orientation is generally described by the Hermans factor:

$$f = \frac{3\langle\cos^2\theta\rangle - 1}{2} \tag{1}$$

where θ is the angle between the chain axis and the chosen reference axis (usually the machine direction). Most samples have a certain degree of symmetry with three orthogonal directions designated as machine (M), transverse (T), and normal (N). For polyethylene, the orientation functions for the a, b, and c crystallographic axis are defined as:

$$f_a = (3\cos^2\alpha - 1)/2 \tag{2a}$$

$$f_b = (3\cos^2\beta - 1)/2 \tag{2b}$$

$$f_c = (3\cos^2\gamma - 1)/2 \tag{2c}$$

where α, β, γ are the angles between the unit whose orientation is of interest (a-axis, b-axis or c-axis) and a reference axis (M, T or N). The three crystallographic axes are perpendicular such that:

$$f_a + f_b + f_c = 0 \tag{3}$$

In many cases, including amorphous polymers, the polymer structural units may be considered as having rotational symmetry around the chain axis and the distribution between the a and b axes can be neglected. PET can be thought to belong to this situation, so it is sufficient to describe the orientation of the chain axis c.

Stein [32,33] proposed the equations to represent biaxial orientation, these were subsequently modified by White and Spruiell [34,35] and the resulting equations are most commonly used today to describe the biaxial orientation state of blown films [34–36].

The orientation and lamellar morphology of the blown polyethylene films have been extensively investigated [37–45], a detailed orientation characterization of LDPE blown films was performed by Cole and Ajji [38]. The row-nucleated crystalline structure first proposed by Keller et al. [37] has been widely accepted to describe the orientation of blown PE films. The crystalline lamellar overgrowth occurs epitaxially from the oriented extended chains. The crystallization of ordered polyethylene is nucleated along some extended chains or bundle of chains. In the extreme case of a high fraction of extended chains prior to crystallization, a highly extended chain-crystal morphology, such as shish kebab, can be formed. In blown films, crystalline lamellae are believed to grow laterally from the extended chain nuclei, with nucleation density depending on the imposed stress. Low stress often results in lamellar growing laterally outward in the form of twisted ribbons with the growth direction parallel to b-axis and a preferential orientation of the a-axis parallel to MD, named Keller–Machin I structure. High stress produces so called Keller–Machin II [37] in which the radially grown lamellae extend directly outward without twisting and generally c-axis orients toward MD. Although many studies concerning the structure of PE blown films were reported [38–45], the knowledge of the detailed crystalline morphology and orientation is still not sufficient to develop a structure–property correlation. In addition, there are few publications concerning the orientation of the amorphous phase for the PE films [46,47].

Numerous studies [48–50] on the orientation of PET can be found in literature. Its orientation was found to be associated with conformational changes. Most of the investigations focused on PET fibers, sheets, bottles, and stretched films, no study can be found on blown PET films. Whether the blowing process can induce a significant orientation and crystallinity level in PET is still unknown.

In the present work, multilayer LDPE/PET blown films were prepared. Ethylene-co-glycidyl methacrylate copolymer (EGMA) was used as a tie layer. The orientation, morphology and crystallization behavior were studied extensively. The objective is not only to evaluate the effect of the tie layer, but also to study the effect of selected processing variables, such as BUR, DDR and the frost-line height, on molecular orientation as well as their influence on the crystallinity and crystalline morphology.

2. Experimental

2.1. Materials and film preparation

Extrusion grade PET was obtained from Dupont (Selar PT 7086), its molecular weight determined by GPC were $M_n = 28,800$ and $M_w = 54,600$. Novapol LF-Y819-A LDPE film resin with density of 0.92 g/cc and melt flow index of 0.75 g/10 min obtained from Nova Chemicals was used. Ethylene-co-glycidyl methacrylate (EGMA) random copolymer (Lotader AX8840) with 8 wt% GMA contents and melt index of 5 g/10 min obtained from ElfAtochem was used as a tie layer to enhance the interfacial adhesion between PET and LDPE.

The multilayer films were prepared by extrusion blowing process. The line obtained from Brampton Engineering consists of five extruders and a stacked die. The extruder zones and die temperatures used are listed in Table 1. Two multilayer systems, with and without the reactive tie layer, were studied in this work. The percentage of each layer was

Table 1
Extrusion temperatures

Extruders (Materials)	Zone 1 (°C)	Zone 2 (°C)	Zone 3 (°C)	Zone 4 (°C)	Die (°C)
A (LDPE)	160	180	180	180	200
B (LDPE or Tie)	160	180	180	180	230
C (PET)	270	300	293	288	271
D (LDPE or Tie)	160	180	180	180	230
E (LDPE)	160	180	180	180	220

fixed, and the compositions and parameter controls are shown in Tables 2 and 3. Two blow-up ratios (BUR) were used, with three DDRs at each BUR. The frost-line height characterizes how fast the stretching is performed. Three frost-line heights were studied for a constant BUR and DDR to evaluate its effect on the structure and properties. DDR and BUR are related as follows:

$$\mathrm{DDR} = \frac{\text{Die gap}}{\text{Film thickness} \times \mathrm{BUR}} \tag{4}$$

So the film thickness changed when BUR (or DDR) changed, the other processing parameters being kept constant.

2.2. Birefringence measurements

The absolute values of birefringence along the machine, transverse, and normal direction were measured by an incident multi-wavelength double beam and photodiode array assembly, combined with an in-house developed software. Detailed set-up of the technique can be found in previous publications [51,52]. The birefringence for our samples was low, so a reference sample with high retardation had to be used. From the measured retardation of the multilayer film, the contribution from LDPE layer and PET layer can be calculated by the method described below, here we assumed the reactive and non-reactive systems have the same optical dispersion.

The light intensity transmitted through a pair of parallel polarizers and the sample is related to the wavelength and birefringence as follows [51]:

$$I \propto \cos^2\left[\frac{\pi \Delta n_0 d}{\lambda} f(\lambda)\right] \tag{5}$$

Table 2
The processing parameters for the systems without tie (each layer composition was fixed as follows: LDPE(33.3%)/LDPE(8.4%)/PET(16.6%)/LDPE(8.4%)/LDPE(33.3%))

Samples	BUR	DDR	Thickness (μm)	Frost-line height (cm)
Ref. 1	1.6	5.2	131	70 ± 10
Ref. 2	1.6	8.6	80	70 ± 10
Ref. 3	1.6	17.5	40	70 ± 10
Ref. 7	2.5	2.7	157	70 ± 10
Ref. 8	2.6	5.4	79	70 ± 10
Ref. 9	2.5	11.1	40	70 ± 10

where Δn_0 is the birefringence constant, d the sample thickness, λ the wavelength, $\Delta n_0 d$ is the so-called retardation. $f(\lambda)$ is the variation of birefringence with wavelength, which depends on the materials structure, it has been proposed to be expressed as [51]:

$$f(\lambda) = \alpha + \frac{\beta}{\lambda^2}\cdots. \tag{6}$$

where β and α are constants determined by the materials structure. The birefringence in the XY plane for a wavelength λ_0 (in most cases $\lambda_0 = 589.6$ nm) can be obtained as:

$$\Delta n_{XY}(\lambda_0) = \Delta n_0 f(\lambda_0) \tag{6a}$$

For the multilayer films containing two or more significantly optically different materials, the dependences of their refractive indexes as a function of wavelength are significantly different, there will be $f_1(\lambda)$, $f_2(\lambda)$,..., each associated with a retardation in the corresponding materials. The cosine argument can be expressed by the following equation:

$$\frac{\pi \Delta n_0 d}{\lambda} f(\lambda) = \frac{\pi d}{\lambda}[\Delta n_{01} f_1(\lambda) + \Delta n_{02} f_2(\lambda) + \cdots] \tag{7}$$

For the LDPE/PET multilayer films, the functions $f_1(\lambda)$ and $f_2(\lambda)$ can be known through regression fitting from previous measurements, $\alpha = 0.9$, $\beta = -4000$, and $\alpha = 0.6$, $\beta = 40,000$ were obtained for PE and PET, respectively. The regressions were made by the in-house developed software, and thus the retardations for each layer can be calculated. To get reliable results, the calculated results were compared with the measured data for the delaminated

Table 3
The processing parameters for the systems with tie (each layer composition was fixed as follows: LDPE(33.3%)/Tie(8.4%)/PET(16.6%)/Tie(8.4%)/LDPE(33.3%))

Sample	BUR	DDR	Thickness (μm)	Frost-line height (cm)
Tie 1	1.6	4.3	160	70 ± 10
Tie 2	1.5	8.9	77	70 ± 10
Tie 3	1.6	17.5	40	70 ± 10
Tie 7	2.6	2.7	157	70 ± 10
Tie 8	2.7	5.5	78	70 ± 10
Tie 9	2.6	10.7	39	70 ± 10
Tie 10	1.9	7.3	61	20 ± 10
Tie 11	1.9	7.2	82	70 ± 10
Tie 12	1.9	7.1	83	120 ± 10

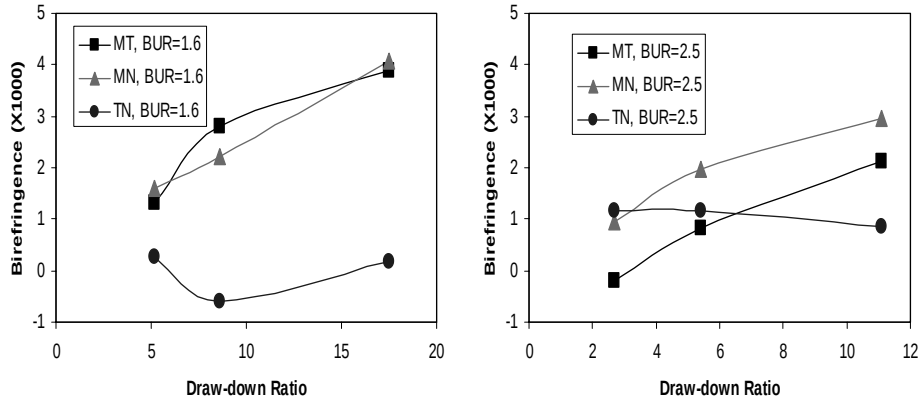

Fig. 1. The plot of birefringence of LDPE layer vs. DDR and BUR, without tie.

layer, and all the calculated retardations were multiplied a corrected coefficient. The different birefringences can be obtained by employing two different incident light angles [51,52]:

$$\Delta n_{MN} = \frac{n}{d(\sin^2\theta_2 - \sin^2\theta_1)}[[\Gamma_1(n^2 - \sin^2\theta_1)^{1/2}] - [\Gamma_2(n^2 - \sin^2\theta_2)^{1/2}]] \quad (8a)$$

$$\Delta n_{MT} = \frac{\Gamma_1}{nd}(n^2 - \sin^2\theta_1)^{1/2} - \frac{\sin^2\theta_1}{n^2}\Delta n_{MN} \quad (8b)$$

$$\Delta n_{TN} = \Delta n_{MN} - \Delta n_{MT} \quad (8c)$$

where n is the average refractive index. θ_1 and θ_2 are the angles between the normal to the MT plane and the incident light beam, Γ_1 and Γ_2 are the retardation at angle θ_1 and θ_2, respectively. The sign of retardation was determined by comparing their values at different angles [51,52].

2.3. Fourier transform infrared spectroscopy

To understand the orientation of the blown films, it is necessary to determine their FTIR spectra corresponding to the machine (M), transverse (T) and normal (N) directions. M and T spectrum (S_M and S_T) can be easily obtained by using a plane-polarized beam with the electric vector in the desired direction. For example, specimen were put perpendicular to the FTIR beam with the machine direction vertically and transverse direction horizontally, and the measurements were performed with the polarization in the M and T direction, respectively. This allows the determination of S_M and S_T. The normal spectrum was obtained using the tilted method [38,53,54], i.e. the films were tilted by 45°, and S_N was calculated by following expression [38]:

$$S_N = \frac{\cos\beta}{\sin^2\beta}(S_{TN} - S_T\cos\beta) \quad (9)$$

where

$$\sin\beta = \frac{\sin 45^\circ}{n} \quad (9a)$$

and

$$S_{TN} = \frac{(S_T\cos^2\beta + S_N\sin^2\beta)}{\cos\beta} \quad (9b)$$

where n is refractive index of the polymer. Because of the

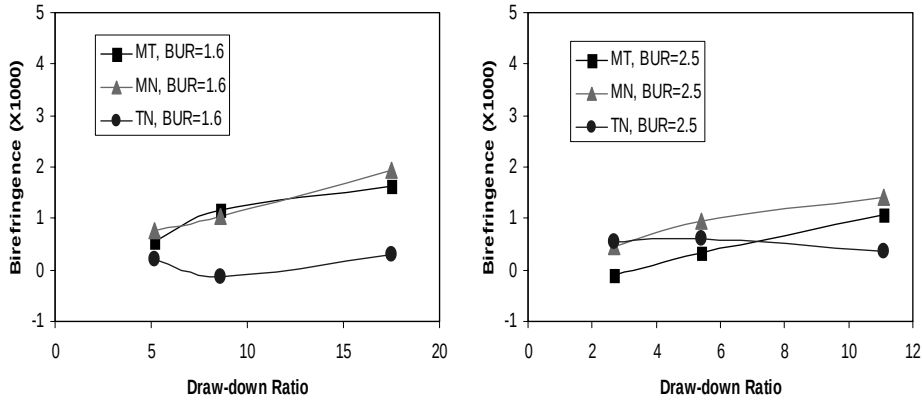

Fig. 2. The plot of birefringence of PET layer vs. DDR and BUR, without tie.

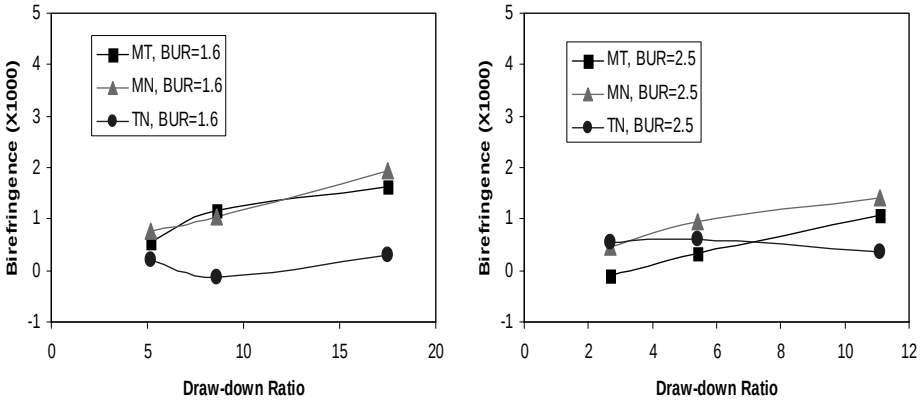

Fig. 3. The comparison of the birefringence for systems with and without tie layer.

refraction, the beam pass through the sample at an angle β, as defined in Eq. (9a). For LDPE,

$$S_N = 4.02930(S_{TN} - 0.88358S_T) \tag{10a}$$

and for PET

$$S_N = 4.46489(S_{TN} - 0.89427S_T). \tag{10b}$$

The isotropic spectrum was calculated by:

$$S_0 = 1/3(S_M + S_T + S_N) \tag{11}$$

Measurements were carried out on a Nicolet 170SX FTIR at a resolution of 4 and 2 cm^{-1} with an accumulation of 128 scans. Polarization of the beam was done by a zinc selenide wire grid polarizer from Spectra-Tech. The spectra were recorded with the plane of polarization parallel and perpendicular to the draw-direction with tilted angles 0 and 45°, respectively.

The multilayer samples without tie could be delaminated so easily that the delamination process cannot produce any influence on the structure. FTIR spectra for the delaminated PET and LDPE layers were collected. The delamination of the multilayer films with tie layer must be done carefully to ensure the process do not initiate any orientation.

2.4. Crystallinity

Initially the crystalline content was studied using Perkin Elmer DSC Pyris1 for both PET and LDPE. A heating rate of 10°C/min was used for the ordinary DSC scan. The crystallinity and cold crystallization temperature were obtained. The enthalpy of fusion of fully crystallized PET was taken as 140 J/g [55], and a value of $\Delta H_0 = 289$ J/g was employed for LDPE [56]. Dynamic DSC (DDSC), in which a specimen is subjected to a heating mode composed of a steady heating with a periodic isothermal run, was also used to determine the crystallinity of PET. A heating rate of 2°C/min and a 60 s isothermal scan were used in this work. The deconvolution of the net heat flow gives the total heat flow obtained from the conventional DSC, but also separates it into heat capacity-related (reversing) and kinetics-related (non-reversing) components [57]. The difference between the two yields the precise initial crystallinity of PET.

2.5. Morphology of the films

To observe the lamellar arrangement of the LDPE layer, an etching method proposed by Bassett [58] was employed. Delaminated LDPE films were dissolved in a 0.7% solution of potassium permanganate in a mixture of equal volumes of orthophosphoric and sulfuric acid. Care must be taken in the

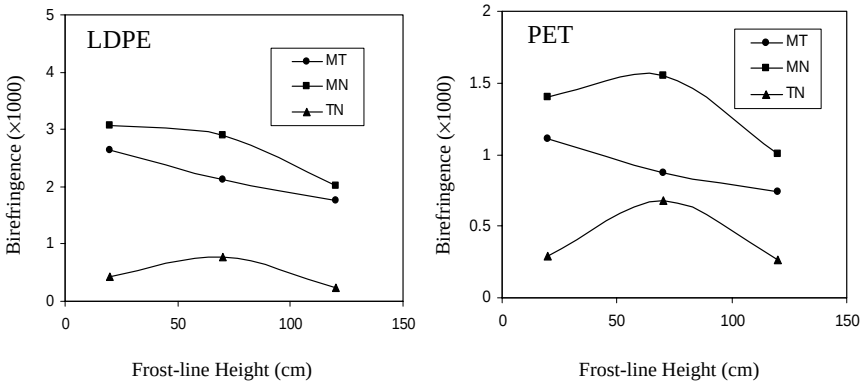

Fig. 4. The plot of birefringence vs. frost-line height with the fixed BUR = 1.9 and DDR = 7.3.

mixing and handling of permanganate reagent, which is a potentially explosive oxidizing agent. The potassium permanganate was slowly added to the sulfuric acid with rapid agitation, not vice versa, in order minimize the likelihood of formation of the unstable and explosive manganese heptoxide. At the end of the reaction time, it was washed as described in Ref. [58]. The use of etching on oriented films must be careful since it may lead to a change of structure. So a series of etching periods (20, 60, 90, 120, 180, 240 min) were employed. It was found for the samples used in this study that there is no influence of the etching time on the morphology if the etching is below 2 h, some effect was observed with 3 and 4 h of etching. So in the present study 20 min of etching was employed instead of 1 h used by Bassett [58]. The etching in the present work is supposed to not produce an unexpected change on the structure.

The lamellar morphology was observed using a Jeol JSM-6100 scanning electron microscope. Both sides of the LDPE films were examined with marked machine direction.

3. Results and discussion

3.1. Birefringence

The measured birefringence of LDPE and PET layers without a reactive tie layer are shown in Figs. 1 and 2, respectively. It is observed that, the birefringence magnitudes are relatively small, both LDPE and PET have weak orientation under the processing conditions used in this work. It is to be noted that LDPE layer has a higher birefringence than that of PET at the same processing conditions. By comparing the birefringence values of MN, MT, TN, it is obvious that LDPE layers mainly oriented along the machine direction (MD), and that the MD orientation increased with draw-down ratio. At BUR = 1.6, $\Delta n_{MN} \approx \Delta_{nMT}$ and $\Delta n_{TN} \approx 0$, the global orientation was almost uniaxial along MD. Both Δn_{MN} and Δn_{MT} increased with increasing DDR. At BUR = 2.5, it is seen that both Δn_{MT} and Δn_{MN} are lower than those at BUR = 1.6, and that Δn_{MT} became lower than Δn_{MN}. The uniaxial orientation behavior was no more observed upon increasing BUR to 2.5. The increase of blow-up ratio resulted in more biaxial orientation. A similar conclusion could also be drawn for the systems containing a reactive tie layer, as illustrated in a comparison between two systems shown in Fig. 3. No significant difference could be detected. For example birefringence Δn_{MT} of sample Ref. 2 and Ref. 3 are 2.497×10^{-3} and 3.696×10^{-3}, while their counterparts, Tie2 and Tie3 are 2.802×10^{-3} and 3.901×10^{-3}, respectively. Their difference is within the measurement error of 0.4×10^{-3}.

The effect of frost-line height on the birefringence was studied for the systems with the reactive tie. Three frost-line heights were used with constant DDR and BUR, and the results are given in Fig. 4. A decrease in Δn_{MT} is observed by increasing the frost line height. In general, a reduction of orientation as the frost-line height increased was observed due to the relaxation of the oriented structure.

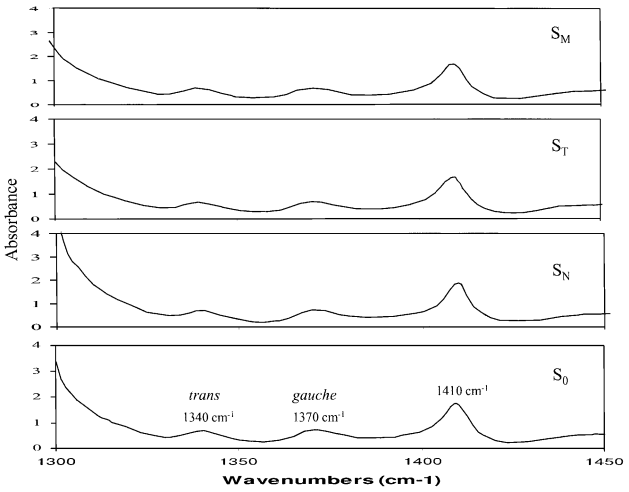

Fig. 5. FTIR spectra for PET layer in Ref. 8 with BUR = 2.5, DDR = 5.4.

3.2. Structure characterization of PET layer by FTIR

Orientation measurements were also carried out using FTIR. The bands used for determination of orientation of the PET layer were those in the range of 1300–1500 cm^{-1} as shown in Fig. 5. The bands at 1340 and 1370 cm^{-1} are assigned to CH_2 wagging modes of the glycol segments possessing the *trans* and *gauche* conformations, respectively [59]. The very low peak intensity at 1340 cm^{-1} indicated the low *trans* conformation fraction and a very low crystallinity level of PET formed in the blowing process. It is well known that the orientation of PET is related with conformational changes about the C–O–C bonds in the ethylene glycol moiety of the repeat unit. The crystalline phases consist solely of the *trans* conformers, whereas both

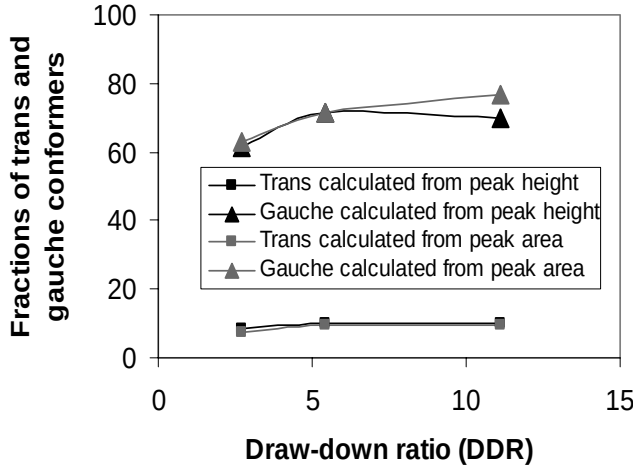

Fig. 6. The fractions of *trans* and *gauche* conformers of PET layer vs. DDR at BUR = 2.5 for the systems without tie.

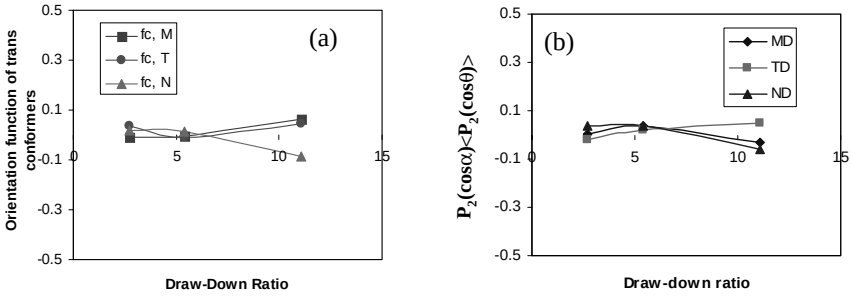

Fig. 7. The orientation function of the *trans* and *gauche* conformers of PET layer vs. DDR at BUR = 2.5 for the system without tie (a) *trans* conformation at 1340 cm^{-1} (b) *gauche* conformation at 1370 cm^{-1}.

of *trans* and *gauche* are present in the amorphous domains [59].

In order to follow the conformational changes, it is required to determine the relative concentrations of both conformers. The calculation was done using the structural factor representing an isotropic sample, which can be easily obtained by $S_0 = 1/3(S_M + S_T + S_N)$. The structural factor was used to measure the peak height or area of the reference, *gauche* and *trans* peaks at 1410, 1370 and 1340 cm^{-1}, respectively. The absorbances were normalized relative to the peak at 1410 cm^{-1}. When A_{1340}/A_{1410} is plotted against A_{1730}/A_{1410}, a straight line with negative slope is obtained, its *x* and *y* intercepts are considered to correspond, respectively to 100% *gauche* and 100% *trans* conformer. Thus the *trans* and *gauche* fractions can be calculated. It is impossible to obtain the straight line for the present study since A_{1340}/A_{1410} and A_{1730}/A_{1410} were almost the same for different samples. According to literature [60,61], values for the peak height ratios of $H_{1340}/H_{1410} = 2.05$ for 100% *trans* and $H_{1370}/H_{1410} = 0.365$ for 100% *gauche* values were obtained. Applying these values, the fractions of *trans* and *gauche* isomers were estimated and presented in Fig. 6. The sum of *trans* and *gauche* obtained is around 0.8–0.90, thus the error is about 10–20%. Nevertheless, it is seen that the fraction of *trans* isomers is very low and does not change with processing conditions.

The orientation functions of the chain axis with respect to a given sample direction J (J = M, T, or N) can be calculated from the dichroism of a specific peak in the IR spectra by [38]:

$$A_J = A_0\{1 + 1/2(3\langle\cos\theta_{cJ}\rangle - 1)(3\cos2\alpha - 1)\}$$

$$= A_0\{1 + f_{cJ}(3\cos^2\alpha - 1)\} \quad (12a)$$

$$f_{cJ} = \{A_J/A_0 - 1\}/[3\cos^2\alpha - 1] \quad (12b)$$

where A_0 represents the absorption intensity for the unoriented sample in the structural factor spectrum, and A_J is the spectrum peak intensity for J direction, α is the angle that the transition moment of the vibration giving rise to the peak makes with respect to the chain axis. The angle is 21° for the peak at 1340 cm^{-1} and 34° for the peak at 970 cm^{-1} [59]. The peak at 970 cm^{-1} was broad and weak, thus only the band at 1340 cm^{-1} was used for the calculation of *trans* orientation. The orientation functions calculated using the peak at 1340 cm^{-1} are shown in Fig. 7(a), they were found to be close to zero, indicating a negligible orientation of

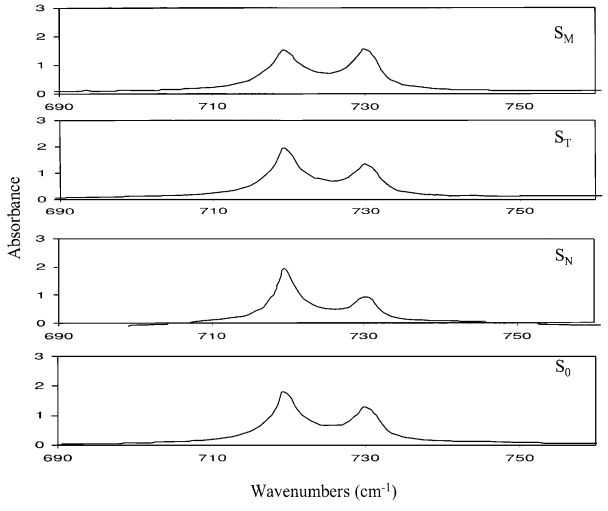

Fig. 8. CH_2 rocking band of LDPE layer in Ref. 1 with BUR = 1.6 and DDR = 5.2.

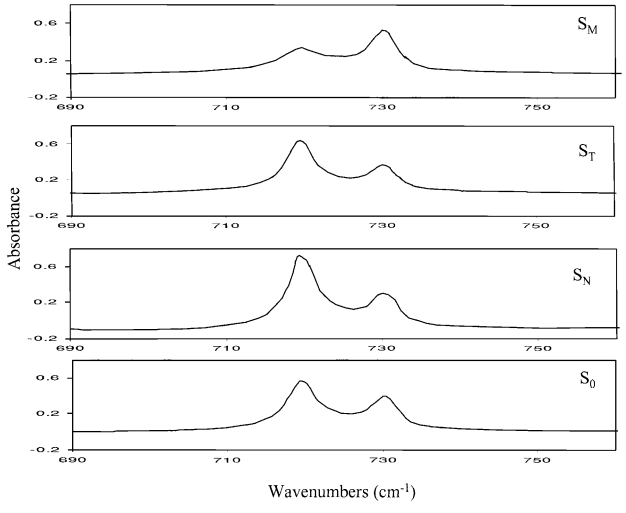

Fig. 9. CH_2 rocking band of LDPE layer in Ref. 3 with BUR = 1.6 and DDR = 17.5.

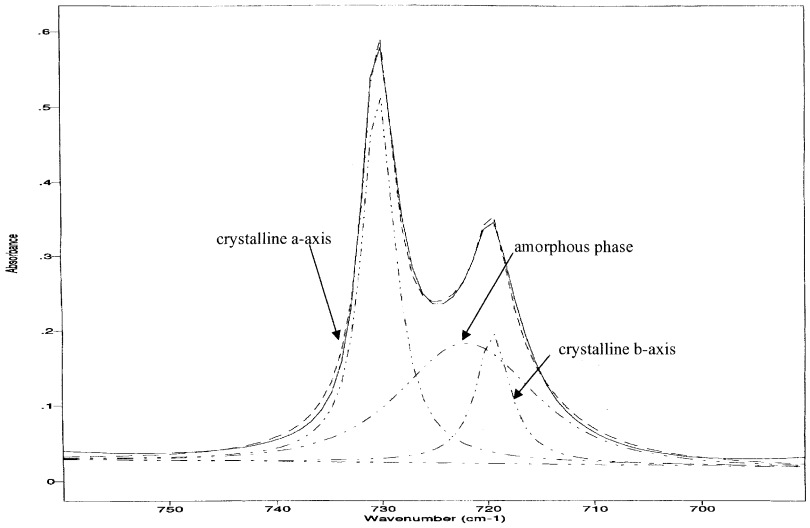

Fig. 10. The decomposition of the band between 700–750 cm^{-1} into three components: crystalline *a*-axis, *b*-axis, and amorphous phase.

trans conformers. Because of the lack of knowledge of the angle α for 1370 cm^{-1}, it is convenient to describe the orientation factors of the *gauche* conformer in terms of the following quantity [38,62–63], which is proportional to the orientation factor f_{cJ}:

$$P_2(\cos\alpha)\langle P_2(\cos\theta)\rangle = [1/2(3\cos^2\alpha - 1)]f_{cJ} = 1/2\{A_J/A_0 - 1\} \quad (13)$$

where α is the angle between the transition moment vector and unit direction, and θ is the angle between the unit direction and a reference axis. This quantity is shown in Fig. 7(b), and it also indicates a negligible orientation of *gauche* conformation. Previous studies have also shown that the *gauche* conformation make a negligible contribution to the overall orientation of PET [62,63]. Thus the PET layer is not significantly oriented for all processing conditions used.

3.3. Structure characterization of LDPE layer by FTIR

The peaks between 710–740 cm^{-1} were employed to analyze the orientation behavior of LDPE layer. Typical absorption spectra are given in Figs. 8 and 9. At low DDR (Fig. 8), the three spectra in MD, TD and ND did not show a significant difference, while MD, TD and ND spectra were quite different at a higher DDR (Fig. 9), confirming the different orientation characteristics with respect to the three directions. The peak at 730 cm^{-1} whose transition moment is parallel to the crystalline *a*-axis [38,64], was strong in M spectra, indicating the *a*-axes were preferentially oriented towards the machine direction. The peak at 720 cm^{-1} whose transition moment is parallel to the crystalline *b*-axis, was weak in the machine direction and strong in the transverse–normal plane. Below the two narrow peaks of crystalline *a* and *b*-axes is the abroad peak at 722 cm^{-1} arising from the contribution of the amorphous phase [64,65].

A spectra curve fitting approach proposed by Cole [38,65]

Table 4
Orientation functions obtained from the analysis of CH_2 rocking band analysis

Sample	Crystalline Phase									Amorphous Phase		
	a-axis (730 cm^{-1})			*b*-axis (719 cm^{-1})			*c*-axis (calculated)			*c*-axis (720 cm^{-1})		
	f_M	f_T	f_N	f_M	f_T	f_N	f_M	f_T	f_N	f_M	f_T	f_N
Ref. 1	0.116	0.001	−0.117	−0.121	0.045	0.076	0.006	−0.046	0.041	−0.104	−0.037	0.142
Ref. 2	0.179	−0.023	−0.156	−0.190	0.149	0.041	0.011	−0.126	0.115	−0.113	0.014	0.099
Ref. 3	0.164	−0.100	−0.064	−0.317	0.098	0.220	0.153	0.003	−0.155	−0.053	0.099	−0.047
Ref. 7	0.020	0.033	−0.054	−0.037	−0.048	0.085	0.017	0.015	−0.032	−0.093	−0.099	0.192
Ref. 8	0.040	−0.017	−0.023	−0.112	−0.008	0.120	0.072	0.025	−0.097	−0.157	−0.047	0.203
Ref. 9	0.108	−0.118	0.010	−0.318	0.048	0.270	0.210	0.070	−0.280	−0.251	−0.192	0.059
Tie 10	0.146	−0.013	−0.133	−0.212	0.034	0.178	0.065	−0.021	−0.044	−0.001	0.065	−0.064
Tie 11	0.118	−0.036	−0.083	−0.212	0.039	0.174	0.094	−0.003	−0.091	−0.116	−0.021	0.136
Tie 12	0.076	−0.004	−0.072	−0.108	0.021	0.087	0.032	−0.017	−0.015	−0.076	−0.036	0.112

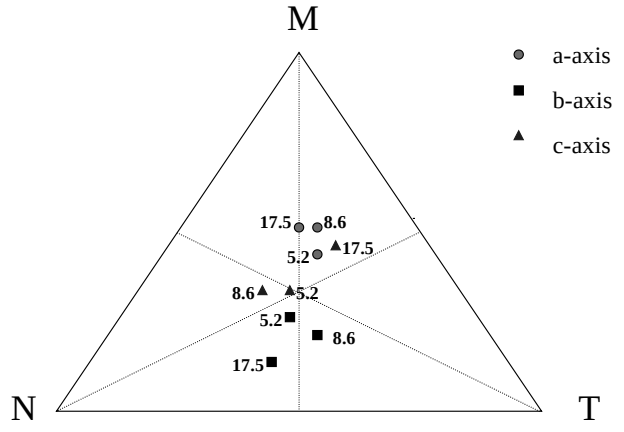

Fig. 11. Orientation functions of crystal phase of LDPE layer with BUR = 1.6 without tie.

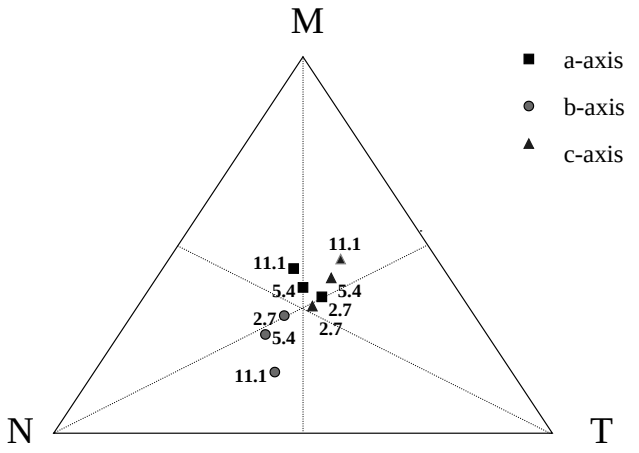

Fig. 12. Orientation functions of crystal phase of LDPE layer with BUR = 2.5 without tie.

was employed to decompose the band into three components corresponding to crystalline *a*-axis, crystalline *b*-axis, and amorphous with the help of BOMEM GRAMS/386 software from Galactic Industries Corp. A typical fitting is shown in Fig. 10. For the crystalline *a*- and *b*-axes of LDPE, the orientation functions f_{aJ} and f_{bJ} with respect to the direction J (J = M, T, or N) were calculated by:

$$f_J = 1/2[A_J/A_0 - 1] \quad (14)$$

The orientation function of crystalline *c*-axis was determined from:

$$f_{aJ} + f_{bJ} + f_{cJ} = 0 \quad (15)$$

The transition moment is perpendicular to the chains axis for the amorphous phase, so its orientation is given by:

$$f_J = 1 - A_J/A_0 \quad (16)$$

The calculated Herman's orientation functions for crystalline *a*-, *b*-, *c*-axes and amorphous phase were listed in Table 4. The measurement error for orientation functions from dichroism in this study was found to be below 0.025. The crystalline *a*-axis orientation was observed to be along the machine direction, the orientation of the crystalline *b*-axis was mainly toward ND and TD, while the *c*-axis oriented along MD at high DDR. The determination of the peak area for amorphous peak was somewhat less precise since it was located under the other two peaks and could be more influenced by interference fringes. The calculated orientation function of amorphous phase was not as precise as that of crystalline phase [38]. Even so, for two series of the samples tested at the two BURs, the same trend can be observed: as DDR increases the orientation of the amorphous phases changed from relatively strong in ND at low DDR to strong in TD at high DDR, while in all conditions no orientation of amorphous phase was observed along MD.

The representation of the orientation results of the LDPE film is performed using the triangle plot with three apices corresponding to perfect orientation in MD, TD and ND and the center corresponding to zero orientation. They are shown in Figs. 11–12, with the digital numbers indicating DDRs. At BUR = 1.6, the crystalline *a*-axis uniaxially oriented toward MD, the crystalline *b*-axis located in the TD–ND plane, and *c*-axis did not show a clear trend but oriented along MD at high DDR. With BUR = 2.6, Fig. 12,

Table 5
Orientation function and birefringence obtained from the global analysis of CH_2 rocking band instead of decomposing it into three components

Sample	Global analysis 750–700 cm^{-1}							
		Orientation function			Order parameters		Birefringence(× 1000)		
	MD/TD	f_M	f_T	f_N	P_{200}	P_{220}	Δn_{MT}	Δn_{MN}	Δn_{TN}
Ref. 1	0.965	0.0063	−0.0300	0.0236	0.0063	−0.0089	1.4	−0.7	−2.1
Ref. 2	0.930	−0.0098	−0.0855	0.0953	−0.0098	−0.0301	2.9	−4.1	−7.0
Ref. 3	0.891	0.1213	0.0014	−0.1352	0.1213	0.0248	4.2	9.9	5.8
Ref. 7	1.000	−0.0490	−0.0489	0.0979	−0.0490	−0.0245	0.0	−5.7	−5.7
Ref. 8	0.981	0.0018	−0.0179	0.0161	0.0018	−0.0057	0.8	−0.6	−1.3
Ref. 9	0.955	0.1106	0.0691	−0.1797	0.1106	0.0415	1.6	11.2	9.6
Tie 10	0.937	0.0678	0.0054	−0.0733	0.0678	0.0131	2.4	5.5	3.0
Tie 11	0.946	0.0209	−0.0349	0.0140	0.0209	−0.0081	2.2	0.3	−1.9
Tie 12	0.969	−0.0128	−0.0452	0.0580	−0.0128	−0.0172	1.3	−2.7	−4.0

a biaxial orientation of *a*-axis along MD and TD was observed at low DDR and it changed to MD as DDR increased, *b*-axis showed a tendency toward ND at low DDR and tended to ND and TD biaxial orientation at high DDR, and the *c*-axis showed some biaxially MD and TD orientation with a tendency to MD at high DDR. As noted in Table 4, a higher *c*-axis orientation value of Ref. 9 than that of Ref. 3 indicated that DDR and BUR interacted and influenced the *c*-axis orientation in a complicated way.

A global analysis of the CH_2 rocking band was tabulated in Table 5, the total area was used instead of decomposing it into three peaks. Orientation functions obtained here are average orientation or so called global orientation. Order parameter P_{2mn} and the calculated birefringence were also included in Table 5. It showed that relative strength of the average orientations in MD, TD and ND were dependent on DDR and BUR. The preferred average orientation was toward MD at high DDR.

Due to the effect of frost-line height the orientation (Fig. 13) showed that the *a*-axis and *b*-axis orientation decreased with increasing frost-line height. Globally, the average orientation tended to be random as frost-line height goes up.

Birefringence concerns the total (crystalline and amorphous) orientation, infrared dichroism can selectively relate the orientation in both amorphous and crystalline phases as well as average (global) orientation. The birefringence can be calculated from FTIR results using the following equations [38]:

$$\Delta n_{MN} = n_M - n_N = \Delta_0(P_{200} + 2P_{220}) + \delta_0(3P_{202} + P_{222}) \quad (17a)$$

$$\Delta n_{MT} = n_M - n_T = \Delta_0(P_{200} - 2P_{220}) + \delta_0(3P_{202} - P_{222}) \quad (17b)$$

$$\Delta n_{TN} = n_T - n_N = \Delta_0(4P_{220}) + \delta_0(2P_{202}) \quad (17c)$$

where P_{2mn} designates the order parameters obtained from calculation of orientation functions and are presented in

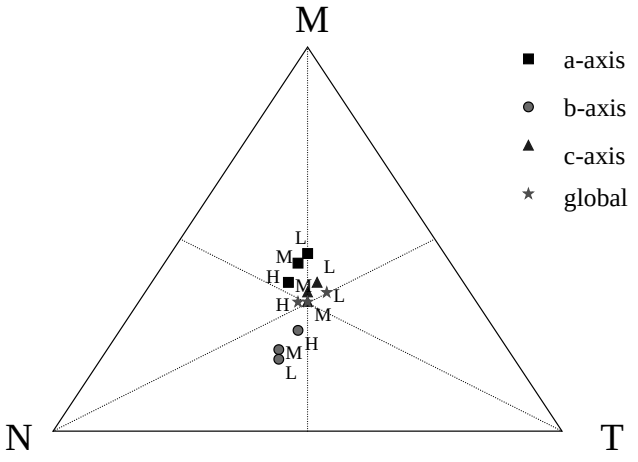

Fig. 13. The crystalline phase and average orientation functions of LDPE layer with three frost-line heights ($H = 120$ cm, $M = 70$ cm, $L = 20$ cm) and fixed BUR = 1.9, DDR = 7.3, with tie.

Table 6. The intrinsic birefringence of both crystalline phase (Δ_0) and amorphous phase (δ_0) of PE were reported as 0.058 [66] and −0.003 [19], respectively.

To determine the importance of the amorphous phase orientation, three approaches [38] were employed to calculate the birefringence from FTIR results. The first one was based on the average orientation of crystalline and amorphous phases which were calculated from the detailed analysis of the decomposed peaks of CH_2 rocking with the help of crystallinity measured by DSC. The second one was assumed no orientation in amorphous phase and the birefringence comes only from the contribution from the crystalline phases. The third approach used the global analysis of CH_2 rocking band, i.e. the total peak area between 750–700 cm^{-1} instead of separating it into 3 peaks. The calculation results are shown in Table 7. All the calculated birefringences showed a similar trend to the measured one, but those calculated from the approach assuming no orientation in amorphous phase were the closest one to the measured birefringence. This supports the fact that the major orientation contribution comes from the crystalline

Table 6
Order parameters obtained from the detailed analysis of CH_2 rocking analysis

Sample	CH_2 rocking P parameter					
	Crystalline Phase				Amorphous Phase	
	P_{200}-Crystal	P_{220}-Crystal	P_{202}-Crystal	P_{222}-Crystal	P_{200}-Amorphous	P_{220}-Amorphous
Ref. 1	0.0056	−0.0145	0.0395	0.0249	−0.1042	−0.0298
Ref. 2	0.0112	−0.0402	0.0615	0.0043	−0.1128	−0.0140
Ref. 3	0.1530	0.0263	0.0800	0.0141	−0.0526	0.0245
Ref. 7	0.0172	0.0078	0.0096	0.0367	−0.0928	−0.0484
Ref. 8	0.0722	0.0204	0.0254	0.0223	−0.1567	−0.0417
Ref. 9	0.2100	0.0583	0.0711	0.0155	−0.2508	0.0223
Tie 10	0.0653	0.0039	0.0597	0.0439	−0.0008	0.0215
Tie 11	0.0941	0.0147	0.0551	0.0304	−0.1159	−0.0261
Tie 12	0.0318	−0.0004	0.0305	0.0225	−0.0762	−0.0246

Table 7
Comparison between the calculated birefringence by IR and measured birefringence

Sample	Calculated birefringence (CH_2 rocking) × 1000															Measured birefringence (× 1000)		
	Crystalline + Amorphous									Without Amorphous			Global analysis 750–700					
	MT crys	MN crys	TN crys	MT amor	MN amor	TN amor	MT aver	MN aver	TN aver	MT aver	MN aver	TN aver	MT aver	MN aver	TN aver	MT mea	MN mea	TN mea
Ref. 1	1.7	−1.8	−3.5	−2.6	−9.5	−6.9	−1.1	−6.8	−5.7	0.6	−0.6	−1.2	1.4	−0.7	−2.1	1.3	1.6	0.3
Ref. 2	4.8	−4.6	−9.4	−4.9	−8.2	−3.3	−1.6	−7.0	−5.3	1.6	−1.6	−3.2	2.9	−4.1	−7.0	2.8	2.2	−0.6
Ref. 3	5.1	11	6.0	−5.9	−0.2	5.7	−2.3	3.5	5.8	1.7	3.6	2.3	4.2	9.9	5.8	3.9	4.1	0.2
Ref. 7	0.1	1.7	1.6	0.2	−11	−11	0.2	−6.7	−6.9	0.0	0.6	0.5	0.0	−5.7	−5.7	−0.2	1.0	1.7
Ref. 8	1.7	6.3	4.6	−4.3	−14	−9.7	−2.1	−6.6	−4.5	0.6	2.3	1.7	0.8	−0.6	−1.3	0.8	2.0	1.2
Ref. 9	4.8	18	13.4	−7.1	−12	5.2	−10	−2.1	7.9	1.6	5.9	4.4	1.6	11.2	9.6	2.1	3.0	0.9
Tie 10	2.9	3.6	0.6	−2.5	2.4	5.0	−1.0	2.8	3.7	0.8	1.0	0.2	2.4	5.5	3.0	2.6	3.1	0.4
Tie 11	3.3	6.6	3.2	−3.7	−9.8	−6.1	−1.1	−3.8	−2.7	1.2	2.4	1.2	2.2	0.3	−1.9	2.2	2.9	0.8
Tie 12	1.7	1.5	−0.2	−1.6	−7.3	−5.7	−0.5	−4.3	−3.8	0.6	0.5	−0.1	1.3	−2.7	−4.0	1.8	2.0	0.2

phase and that the amorphous phase is relatively randomly oriented.

The transition moment at 1368 cm^{-1} band is perpendicular to the chain axis and is associated with the amorphous phase orientation [17,67,68]. This peak has been assigned to molecular segments involving *gauche* conformers presented only in the amorphous phase. From the peak heights of MD, TD and ND spectra in Fig. 14, another value of orientation functions for the amorphous phase can be obtained. For example, f_M, f_T and f_N of sample Ref. 3, with the highest DDR, were calculated as −0.0052, 0.0074, and −0.0023, respectively. These are very low, again, they showed almost no orientation of the amorphous phase.

3.4. Crystallinity and crystallization temperature

The crystallinities of both LDPE and PET layer determined by DSC, it was found that the crystallinity for the LDPE layer does not show any trend with changing DDR and BUR. The crystallinity of PET was observed to range from 10 to 22% from DSC measurements. However, these values for PET are not reliable because it is well known that PET crystallizes very slowly, and during the heating flow of DSC measurement the secondary crystallization may take place. Therefore, it is not accurate to get the initial crystalline percentage of PET by using the traditional DSC technique. The DDSC technique was then used to measure accurately the crystallinity of PET. An example of a DDSC scan is shown in Fig. 15 and it shows the total, reversing and non-reversing heat flows. To calculate the initial crystallinity, the additional crystallinity formed during the heating process has to be subtracted from the total endothermic heat flow. This can be easily done through calculation $\Delta H = (\Delta H_{\text{reversing}} - \Delta H_{\text{non-reversing}})$, where $\Delta H_{\text{reversing}}$ is the endothermic melting enthalpy from the reversing heat flow and $\Delta H_{\text{non-reversing}}$ is the exothermic ordering and cold crystallization enthalpy from the non-reversing heat flow. The crystallinity of PET film was observed to be almost zero for the investigated samples with different conditions, even though the crystallinity of the same film was measured to be as high as 10–22% crystallinity using DSC. From FTIR measurements it was found the *trans* intensity is very low, and comparable with that of quenched PET, indicating that the crystallinity of PET is close to zero.

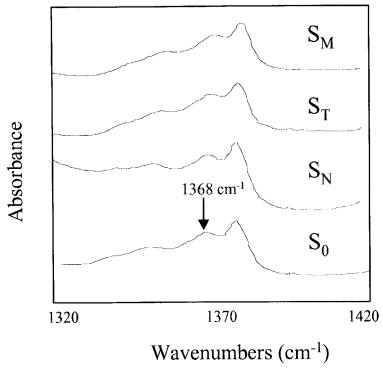

Fig. 14. FTIR spectra of Ref. [3] with BUR = 1.6, DDR = 17.5 at 1368 cm^{-1} band for the amorphous orientation perpendicular to the chain axis.

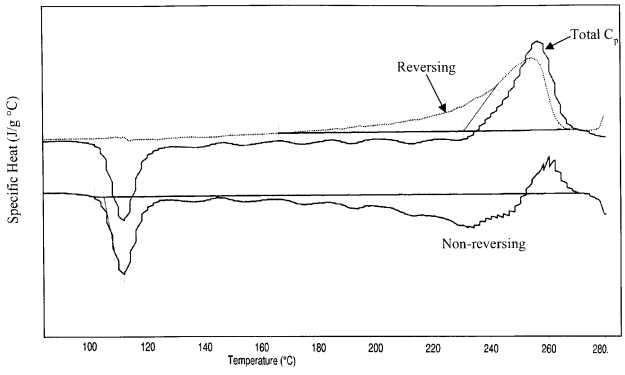

Fig. 15. DDSC scan for a delaminated PET layer of sample Ref. [3] with BUR = 1.6, DDR = 17.5.

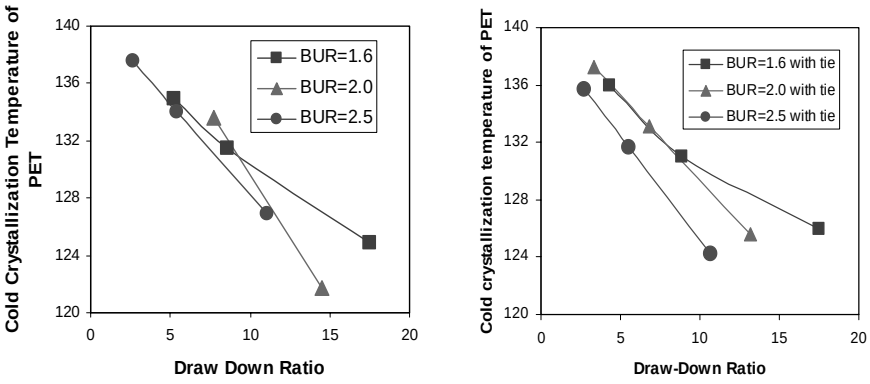

Fig. 16. The cold crystallization temperature of PET as function of BUR and DDR. The PET layer in the multi-layer films without tie (left) and with tie (right).

Nevertheless, it was observed that the cold crystallization temperature of PET decreased with increasing DDR, Fig. 16, and BUR did not have any significant influence on it. This means that there was some kind of 'ordered' structure in the blown PET films which played the role of a nucleating agent for the cold crystallization, in spite of its negligible orientation and amorphous nature.

The effects of frost-line height on the crystallization temperature of PET and on crystallinity of LDPE are shown in Fig. 17(a) and (b), respectively. An increase in frost-line height resulted in an increase of both the cold crystallization temperature of PET and crystallinity of LDPE. The increase of the frost-line height allowed LDPE to have more time to crystallize, and thus a more perfect crystal structure and an increase of the crystallinity. At the same time, the increase of the frost-line height would somehow destroy the oriented structure through relaxation, leading to the decrease of the LDPE orientation and of the 'ordered' PET amorphous structure (thus an increase of cold crystallization temperature of PET).

3.5. Morphology models

Blown films have a unique morphology that results from the large elongational flow in the melt and the interaction between BUR, DDR and cooling conditions. SEM pictures of etched LDPE layers at BUR = 1.6 with the indicated MD direction are shown in Fig. 18, and a higher magnification in Fig. 19. Lamellae with uniform thickness can be observed in Fig. 18(a) and align randomly along the MD and TD, no so called row-nucleated morphology [37] is observed. In this case, the nucleating sites seem mainly to locate along the film surface. Pazur and Prud'homme [21] found a combination of two morphologies: a surface trans-crystalline and a row-nucleated morphology caused by crystallization under low-stress conditions. As the DDR increased the *a*-axis orientation increased and the lamellae were more inclined to be perpendicular to MD, and a perfect nucleated row structure, such as that proposed by Keller [37] to be the basic process of crystallization under stress or flow, was distinctly found at high DDR, Fig. 18(c). These stacked lamellae were aligned parallel to MD. These columns have a uniform width of about 0.5 μm in each row, it appears like nucleating from a central fibrous nuclei. Some extended-chain or chain-folded crystals lamellae could form in the melt and these would provide the nuclei from which the lateral crystal growth would start. Higher MD stress in the melt caused by increasing DDR seemed to promote formation of fibrous nucleation in blown films and thus the row nucleation at the expense of trans-crystalline morphology. The proximity of nuclei along the rows confined crystal growth to the plane perpendicular to the direction of the stress, lamellar crystal growth was normal to the stress direction. No significant lamellae twist, as

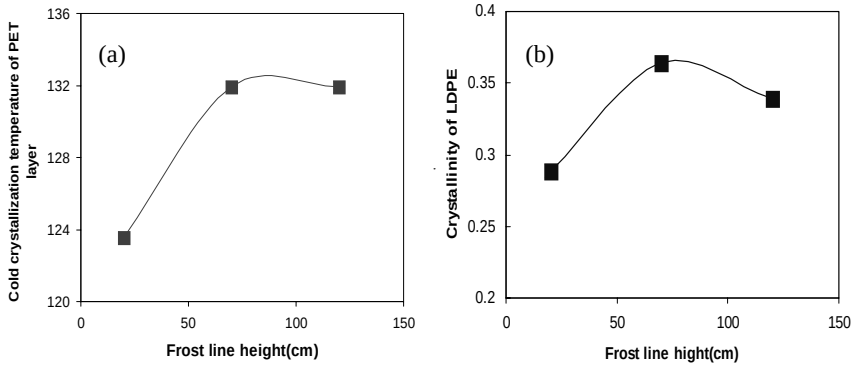

Fig. 17. Effect of frost line height on cold crystallization temperature of PET and crystallinity of LDPE.

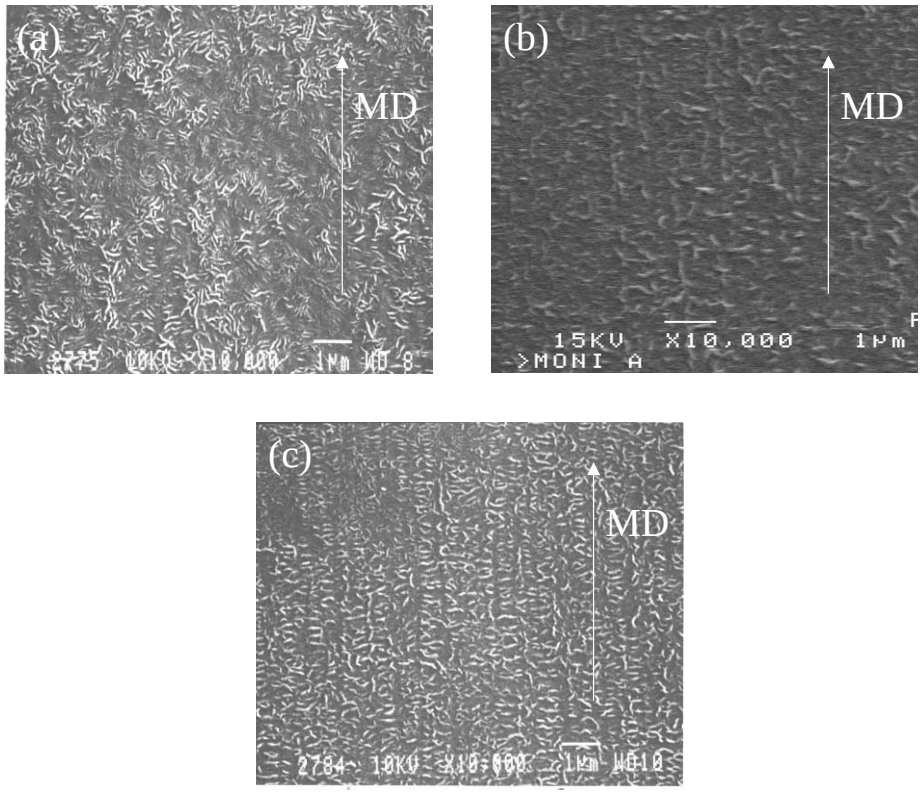

Fig. 18. The dependence of lamellae alignment of LDPE layer on the DDR at BUR = 1.6 (X10,000) (a) Ref. 1 with DDR = 5.2; (b) Ref. 2 with DDR = 8.6; (c) Ref. 3 with DDR = 17.5.

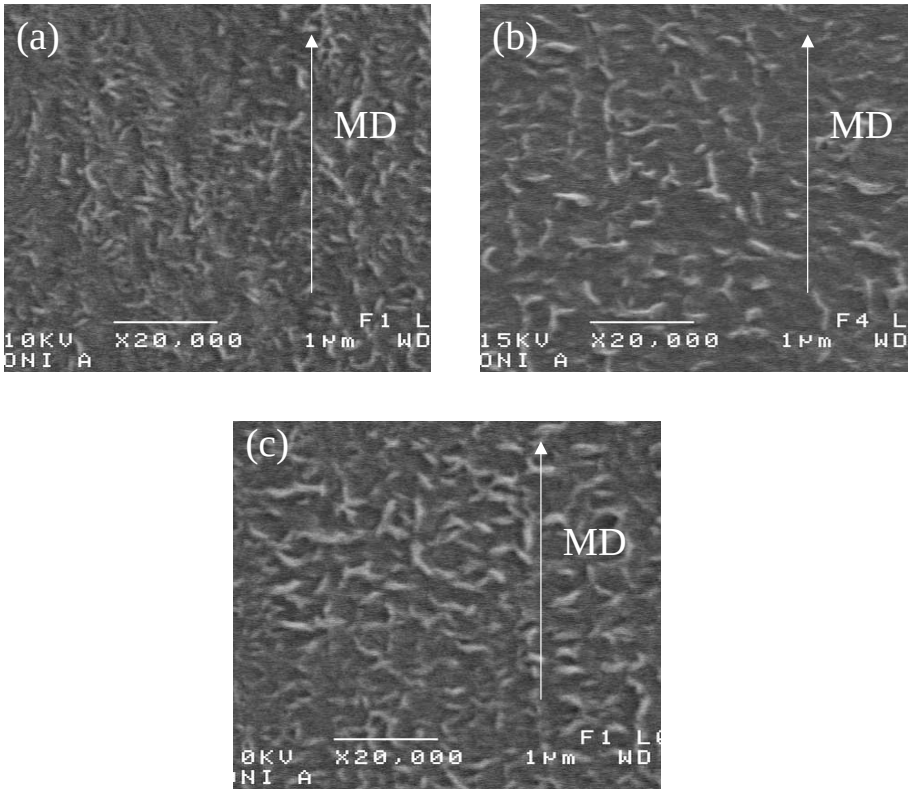

Fig. 19. The dependence of lamellae alignment of LDPE layer on the DDR at BUR = 1.6 (X20,000) (a) Ref. 1 with DDR = 5.2 (b) Ref. 2 with DDR = 8.6 (c) Ref. 3 with DDR = 17.5.

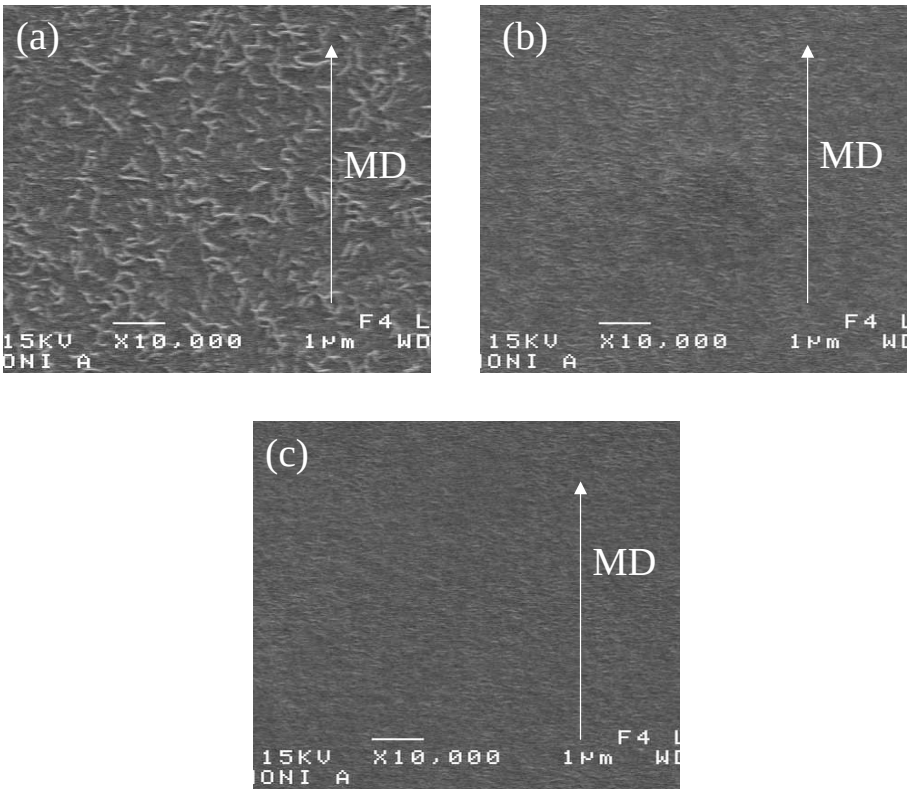

Fig. 20. The dependence of lamellae alignment of LDPE layer on the DDR at BUR = 2.5 (X10,000) (a) Ref. 1 with DDR = 2.7 (b) Ref. 2 with DDR = 5.4 (c) Ref. 3 with DDR = 11.1.

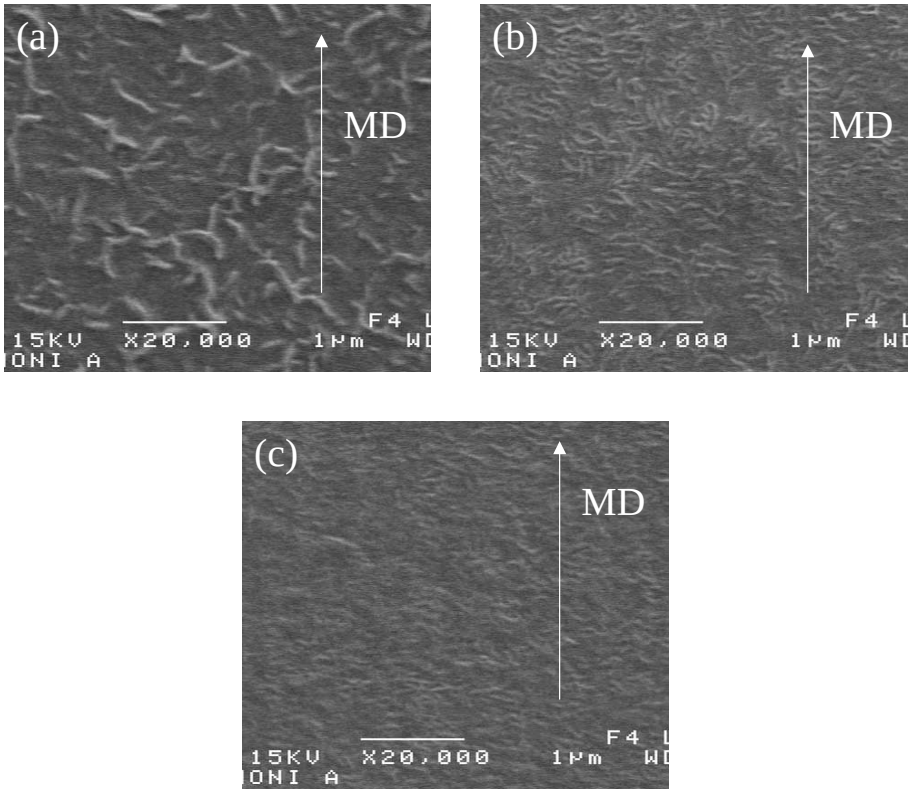

Fig. 21. The dependence of lamellae alignment of LDPE layer on the DDR at BUR = 2.5 (X20,000) (a) Ref. 7 with DDR = 2.7 (b) Ref. 8 with DDR = 5.4 (c) Ref. 9 with DDR = 11.1.

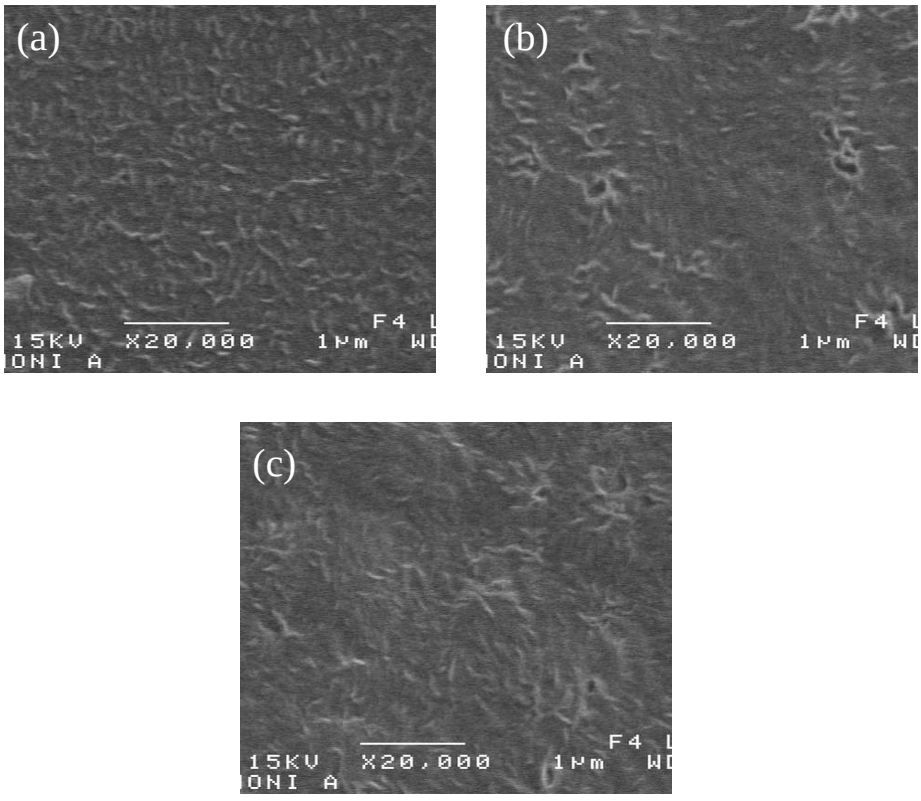

Fig. 22. The dependence of lamellae alignment of LDPE layer on the frost-line height (X20,000). (a) Tie10 with FL = 20 cm. (b) Tie11 with FL = 70 cm. (c) Tie12 with FL = 120 cm.

mentioned in Keller's row nucleation model, can be seen for the samples in this work.

The morphology patterns for BUR = 2.6 with three DDRs are shown in Figs. 20 and 21. The sample with lowest DDR in this series showed a weak and equally balanced orientation with respect to the MD and TD from FTIR and birefringence. The lamellae were found to be not aligned uniformly along MD or TD but curled and interconnected. The balanced biaxial stress in the MD and TD plane would force extended chains and lamellae to become isotropically distributed. No row structure was observable because of the low lamellar orientation. In Figs. 20(b) and 21(b), DDR = 6.8, both *a*-axis orientation along MD and *b*-axis orientation in the plane normal to MD increased, the row nucleation was formed but with a tilted angle toward TD due to the interaction of the stress along TD and MD. Upon cooling, crystallization would occur along these tilted oriented nucleating chains, thus causing the resulting row morphology to be mainly distributed in MD with some kind of tilted angle to TD plane. As DDR further increased, a more perfect row structure was observed, Fig. 20(c) and Fig. 21(c), due to the preponderance of the stress in MD.

The dependence of lamellar structure on the frost-line height is depicted in Fig. 22. Crystallization from the stressed LDPE melt did not produce the familiar randomly nucleated spherulitic crystal structure. Instead, an oriented lamellar or row-nucleated structure was observed at low frost-line height. As the frost-line height was increased, more relaxation time was available for the oriented lamellae, thus partially or completely destroyed the formed orientation. The crystallization style changed from the lamellar growth with a preference to the oriented direction, to the more familiar three-dimensional spherulitic growth style. This morphology change has significant influence on the physical properties, such as the optical properties or mechanical performance.

4. Conclusions

In the LDPE/PET multilayer films, the use of tie layer did not induce any significant change on the structure even though the adhesion was observed to be improved. LDPE and PET behave similar to the behavior expected from their single layer blown counterparts. The PET layer showed an amorphous phase and a negligible orientation formed in the blowing process. Changing the processing conditions mainly resulted in the change of the orientation structure and lamellar morphology of LDPE layer. DDR, BUR and cooling conditions controlled orientation and the crystalline structure of the oriented LDPE melt. Thus for the study of processing–structure–properties relationship, the physical properties of the multilayer films should be correlated

with the orientation structure of LDPE layer. The adhesion kinetics and the correlation between physical properties and structure will be the focus of another separate paper of this series [69].

The orientation of LDPE layer showed that the crystalline *b*-axis was enhanced in TD–ND plane, the crystalline *a*-axis preferentially oriented along MD, and no orientation for the amorphous phase. Globally, the degree of orientation was not as high as crystalline *a*-axis or *b*-axis did, but it had a tendency toward MD at high DDR. Birefringence results indicated an orientation mainly along MD, and at some particular conditions, such as low DDR and high BUR, a biaxial behavior was observed. The crystallization of LDPE melts in the blown films produced lamellar stacks or a morphology consisting of rows of lamellar crystals aligned parallel to the flow direction, it was not always row-nucleated style. The exact pattern depended on the distribution of the crystalline *a*-axis and *b*-axis orientation, which in turn was a function of DDR, BUR and frost line. Low BUR and high DDR favor the formation of the row structure, the increase of BUR decreased the *a*-axis orientation in MD and *b*-axis orientation in TD, thus leading to a tilted row structure. The low frost-line can suppress the relaxation of the oriented lamellar or extended chains, keeping the row/lamellar style morphology, while the high frost-line may lead to the more familiar spherulitic crystalline morphology.

Acknowledgements

The authors are indebted to Dr Kenneth Cole for helpful discussions on the analysis of FTIR results, to Mr Jacques Dufour and Mr Robert Lemieux for the sample preparation by extrusion blowing process. They also wish to thank Mrs Roberge Helene for skillful SEM measurements.

References

[1] Shirodkar PP, Firdaus V, Vickers WE. Plast Engng 1994:27.
[2] Kanai K, Kimura M, Asano Y. Proc SPE ANTEC 1986. p. 912.
[3] Farber R, Dealy J. Polym Engng Sci 1974;14:435.
[4] Simpson DM, Harrison DR. Proc SPE ANTEC 1991. p. 203.
[5] Huang TA, Campbell GA. Adv Polym Technol 1990;5:181.
[6] Babel AK, Campbell GA. J Plast Film Sheet 1993;9:246.
[7] Campbell GA, Babel AK. Macromol Symp 1996;101:199.
[8] Butler TI, Lai SY, Patel R, Spuria J. TAPPI Polymer, Lamination and Coatings Conference 1993. p. 13.
[9] Butler TI, Lai SY, Patel R, TAPPI Polymer, Lamination and Coatings Conference 1993. p. 289.
[10] Sukhadia A. Proc SPE ANTEC 1994. p. 202.
[11] Cao B, Sweeney S, Campbell GA. J. Plast Film Sheet 1990;6:117.
[12] Hauck J, Michaeli W. Proc SPE ANTEC 1998. p. 123.
[13] Feron B, Wolf D, Wortberg J. Proc SPE ANTEC 1996. p. 106.
[14] Akbar G. Plast Film Sheet 1999;15:194.
[15] Chiu DY, Ealer GA, Moy FH, Buhler-Vidal JO. J Plast Film Sheet 1999;15:153.
[16] Simpson DM, Harrison IR. J Plast Film Sheet 1995;11:216.
[17] Yu TY, Wilkes GL. Polymer 1996;37:4675.
[18] McRae MA, Maddams WF. J Appl Polym Sci 1978;22:2761.
[19] Cantor K. Proc SPE ANTEC 2000. p. 341.
[20] Krishnaswamy KR. J Polm Sci, Part B: Polym Phys 2000;38:182.
[21] Pazur RJ, Prud'homme RE. Macromolecules 1996;29:119.
[22] Sukhadia A. Proc SPE ANTEC 1998. p. 160.
[23] Chai CK, Selo JL, Osmont E. Proc SPE ANTEC 2000. p. 331.
[24] Krishnaswamy RK, Lamborn MJ. Proc SPE ANTEC 2000. p. 336.
[25] Ashizawa H, Spruieil JE, White JL. Polym Engng Sci 1984;24:1035.
[26] Han CD. Multiphase flow in polymer processing. London: Academic Press, 1981.
[27] Schrenk WJ, Alfrey T. In: Paul DR, Seymour N, editors. Coextruded multilayer polymer films and sheets in polymer blends, vol. 2. London: Academic Press, 1978.
[28] Morris BA. ANTEC'96, 1996. p. 116.
[29] Morris BA. Proc SPE ANTEC 1998. p. 118.
[30] Saito T, Macosko CW. Proc SPE ANTEC 1998. p. 967.
[31] Ebeling T, Norek S, Hasan A, Hiltner A, Baer E. J Appl Polym Sci 1999;71:1461.
[32] Stein RS. J Polym Sci, Part B: Polym Phys Ed 1958;31:335.
[33] Stein RS. J Polym Sci, Part B: Polym Phys Ed 1961;50:339.
[34] White JL, Spruiell JE. Polym Engng Sci 1981;21:859.
[35] White JL, Spruiell JE. Polym Engng Sci 1983;23:247.
[36] White JL, Cakmak M. Adv Polym Technol 1988;8:27.
[37] Keller A, Machin MJ. J Macromol Sci (Phys) B 1967;1(1):41.
[38] Cole KC, Ajji A. In: Ward IM, Coates PD, Dumoulin MM, editors. Characterization of orientation in solid phase processing of polymers, Munich: Carl Hanser, 2000.
[39] Maddama WF, Preedy JE. J Appl Polym Sci 1978;22:2721 see also p. 2739,2751.
[40] Choi K, Spruiell JE, White JL. J Polym Sci, Part B: Polym Phys Ed 1982;20:27.
[41] Shimomura Y, Spruiell JE, White JL. J Appl Polym Sci 1982;27:2663.
[42] Picot JC. Polym Engng Sci 1984;24:415.
[43] Haber A, Kamal MR. Proc SPE ANTEC 1987. p. 446.
[44] Kwack TH, Han CD. J Appl Polym Sci 1988;35:363.
[45] Simpson DM, Harrison IR. J Plast Film Sheet 1994;10:302.
[46] Patel RM, Butler TI, Walton KL, Knight GW. Polym Engng Sci 1994;34:1506.
[47] Kim Y, Park J. J Appl Polym Sci 1996;61:2315.
[48] Ajji A, Guevremont J, Cole KC, Dumoulin MM. Polymer 1996;37:3707.
[49] Ajii A, Cole KC, Dumoulin MM, Ward IM. Polymer 1997;37:1801.
[50] Guevremont J, Ajji A, Cole KC, Dumoulin MM. Polymer 1996;36:3385.
[51] Ajji A, Guevremont J, Matthews RG, Dumoulin MM Proc SPE. ANTEC1998. p. 1588.
[52] Ajji A, Guevremont J. US Patent No. 5,864,403, 1999.
[53] Koenig JK, Cornell SW, Witenhafer WE. J Polym Sci, Part A-2 1967;5:301.
[54] Kole KC, Ben DH, Sanschagrin B, Nguyen KT, Ajji A. Polymer 1999;40:3505.
[55] Mehta A, Gaur U, Wunderlich B. J Polym Sci, Part B: Polym Phys Ed 1978;16:289.
[56] Mandelkern L. Crystallization of polymers. New York: McGraw-Hill, 1964.
[57] Reading M, Elliott D, Hill VH. J Therm Anal 1993;40:949 see also p. 931.
[58] Olley RH, Bassett DC. Polymer 1982;23:1707.
[59] Spiby R, O'Neill MA, Duckett RA, Ward IM. Polymer 1992;21:4479.
[60] Edelmann K, Wyden H. Kautschuk Gummi-Kunstoffe, 1972, p. 353.
[61] Guevremont J, Ajji A, Cole KC, Dumoulin MM. Polymer 1995;36:3385.
[62] Cunningham A, Ward IM, Willis HA, Zichy V. Polymer 1974;15:749.

[63] Yazdanian M, Ward IM, Brody H. Polymer 1985;26:1779.
[64] Kissin YV. J Polym Sci, Part B: Polym Phys 1992;30:1165.
[65] Cole KC, Legros N, Ajji A. International Symposium On Orientation of Polymers (SPE RETEC), Boucherville, Canada, 1998. p. 322.
[66] Rossignol JM, Seguela R, Rietsch F, Dupuis-Lallemand J. J Polym Sci, Part C: Polym Lett 1989;27:527.
[67] Glenz W, Peterlin A. J Macromol Sci Phys B 1970;4(3):473–90.
[68] Glenz W, Peterlin A. J Polym Sci A2 1971;9:1191.
[69] Zhang XM, Ajji A, Verilhac JM. Polym Eng Sci, submited.